# Research Article

# The Performance-Stability Conundrum of BTP-based Organic Solar Cells

Yunpeng Qin, <sup>1</sup> Nrup Balar, <sup>1</sup> Zhengxing Peng, <sup>1</sup> Abay Gadisa, <sup>1</sup> Indunil Angunawela, <sup>1</sup>Anirban Bagui, <sup>1</sup> Somayeh Kashani, <sup>1</sup> Jianhui Hou, <sup>2\*</sup> Harald Ade<sup>1,3\*</sup>

<sup>1</sup>Department of physics and Organic and Carbon Electronics Laboratories (ORaCEL), North Carolina State University, Raleigh, NC 27695, USA <sup>2</sup>State Key Laboratory of Polymer Physics and Chemistry, Institute of Chemistry Chinese Academy of Sciences, Beijing 100190, China <sup>3</sup>I end contact

\*Correspondence: hjhzlz@iccas.ac.cn, hwade@ncsu.edu

#### **SUMMARY**

As the power conversion efficiency of organic photovoltaic has been dramatically improved to over 18%, achieving long-term stability is now crucial for applications of this promising photovoltaic technology. Among the high-efficiency systems, most are using BTP-4F and its analogs as acceptors. Herein, we determine the thermal transition temperatures ( $T_{\rm g}$ ) of seven BTP-analogs to develop a structure- $T_{\rm g}$  framework. Our results point out an unresolved molecular design conundrum on how to simultaneously achieve high performance and intrinsic stability with BTP-based acceptors. We also show that PC<sub>71</sub>BM has a miscibility above the percolation threshold in PM6 and can maintain local charge percolation and improved stability in ternary devices. However, PC<sub>71</sub>BM is not miscible with BTP-C3-4F and the unfavorable vertical gradients still degrade performance. This points to a second thermodynamic conundrum. A compound with differential miscibility in the donor polymer can only impact percolation, a compound with differential miscibility with the BTP only impacts diffusion.

Keywords: Organic solar cells, stability, glass transition temperature, miscibility

# Context & Scale

Solution-processed organic solar cells (OSCs) utilizing bulk heterojunction (BHJ) architecture have attracted considerable attention for their promise of being low cost and easy to fabricate by large-scale roll-to-roll processing. Particularly, OSCs based on emerging non-fullerene acceptors have enjoyed significant attention in recent years due to dramatically improving efficiency, however, long-term stability is crucial for the practical application of this promising photovoltaic technology and therefore becomes an imperative research goal in the community. Here, we determine the thermal transition temperatures of seven BTP-based nonfullerene acceptors. Using the Gordon-Tayler relations, we have developed a structure- $T_g$ framework that can disentangle the contribution to  $T_{\rm g}$  of the outer (unbranched) and inner (branched) sidechains, as well as the two different cores. We also show that PC71BM has a miscibility above the percolation threshold in PM6 and can thus maintain local charge percolation. However, PC71BM is not miscible with BTP-C3-4F and can thus not prevent BTP-C3-4F diffusion and the development of unfavorable vertical gradients that still degrades performance. In addition to PC71BM, an additional, high Tg component with suitable electronic structures that prevents BTP diffusion would be required to achieve commercial viability.

#### HIGHLIGHTS

- BTP-based OSCs (including the star acceptor BTP-4F) are intrinsically unstable or have low performance
- Molecular designs that yield materials with high glass transition temperatures are needed to achieve long-term OSCs stability
- Alternatively, additives in complex ink formulations that reduce the mobility of BTP-based NFAs are required.

# INTRODUCTION





Organic solar cells (OSCs) based on non-fullerene acceptors (NFAs) have achieved benchmarks that seemed out of reach only a decade ago 1-7. The power conversion efficiency (PCE) has been significantly improved with many reports of 17-18%8-14, and NREL certification of over 18%. The main current strategies for improving the PCE in OSCs are new materials development, and ternary and even quaternary ink formulations consisting of blending multiple donors and/or acceptors while maintaining the single junction configuration<sup>9</sup>, <sup>14</sup>. The higher PCEs achieved are getting closer to the requirement for commercial applications. However, to be commercially viable, an OSC must maintain consistent performance throughout its lifetime. There is a high standard for any new product used in large-scale energy production, as established PV companies that employ materials such as crystalline silicon or cadmium telluride warranty their products for 25 years 15. Although it is estimated that OSCs may only need to retain performance for 10 years to be commercially competitive 16, particularly in various niche markets, achieving that stability poses a significant challenge. In addition, module performance and their stability are important. Thus, it is urgent to demonstrate high-performance, stable large-area OSCs and OSC modules that can be fabricated by scalable printing strategies<sup>17-18</sup>. Despite this need, understanding the various degradation mechanisms lags far behind the rapidly improving PCE19-22. Understanding the intrinsic morphological stability across the families of NFAs such as BTP-4F (Y6), EH-IDTBR, di-PDI, ITIC, IEICO-4F, etc. (for full chemical names of any materials referred to, please see \$10 in the supplemental information), within a family, and particularly of the current star acceptor BTP-4F and its analogs is paramount to further improve or maintain performance while also achieving stability.

Several different degradation mechanisms of OSCs such as oxygen-, water-, or interface assisted photo-reactions<sup>23-26</sup>, electrode degradation<sup>27</sup>, and morphology instability<sup>17, 22, 28-30</sup> can be differentiated. Here we will focus on morphological instability, which predominantly takes the form of i) over-purification of the mixed domains that have been quenched to a composition close to the percolation threshold for optimal performance<sup>31,32</sup>, ii) NFA crystallization<sup>32-34</sup>, and iii) development of an unfavorable gradient or wetting layer<sup>21</sup>. Diffusion directly affects all three pathways, for example the ability of the mixed domains to evolve from the percolation threshold to the binodal after casting. Similarly, high diffusion coefficients lead to higher nucleation density of crystals and faster crystal growth and lower stability<sup>34</sup> or enable vertical redistributions driven by differences in interfacial energies. Our recent work has confirmed that the morphological stability is strongly dependent on the diffusion coefficients of the NFA and, importantly, that the relative diffusion properties and thus morphological stability can be



predicted by proxy metrics such as the glass transition temperature ( $T_g$ ) of the NFA and the elastic modulus ( $E_f$ ) of the donor polymer<sup>35</sup>. This study has also established that PBDB-T/PM6 is the most stable donor family amongst the high performance polymers P3HT, FTAZ, PTB7-th used with NFAs in general. At the same time, it revealed that BTP-4F has the lowest  $T_g$  amongst the NFA investigated (BTP-4F, EH-IDTBR, di-PDI, IT-M, IEICO-4F) and that BTP-4F-binary devices are unstable at room temperature (RT) even when paired with PM6.

We regard it as proven that higher Tg (for similar molecular weight) leads to lower diffusion and more stable devices. We are not seeking to re-establish that known fact, but are interested in establishing molecular structure- $T_g$  relations. We also want to understand the thermodynamic mechanism of success or failure of stabilizing a high-efficiency BTP system with PCBM. Due to this focus on thermodynamics, we briefly provide a context. The miscibility is a parameter that can be significant in determining the final properties of devices including their stability<sup>36-39</sup>. Hyper-miscibility (miscibility above the percolation threshold) leads to low performance due to insufficient phase separation (see the framework as outlined in Figure 1). Hypo-miscibility (miscibility below the percolation threshold) can lead to burnin degradation when the mixed domains of an optimized morphology that were quenched near the percolation threshold are evolving towards the miscibility gap (i.e. binodal). A device with a miscibility gap close to the percolation threshold is expected to exhibit a relatively stable morphology if optimized properly and thus low burn-in degradation<sup>28</sup>. Importantly, very low miscibility systems have high activation energy for diffusion and thus small diffusion coefficients<sup>35</sup>. These systems are thermodynamically highly unstable but are kinetically stabilized as illustrated and conceptualized in Figure 1, in which the miscibility is encoded by the Flory-Huggins interaction parameter χ. Optimized devices have mixed domains with a composition near the percolation threshold, which has to be achieved by kinetically trapping the mixed domains during fabrication<sup>31,32</sup>.



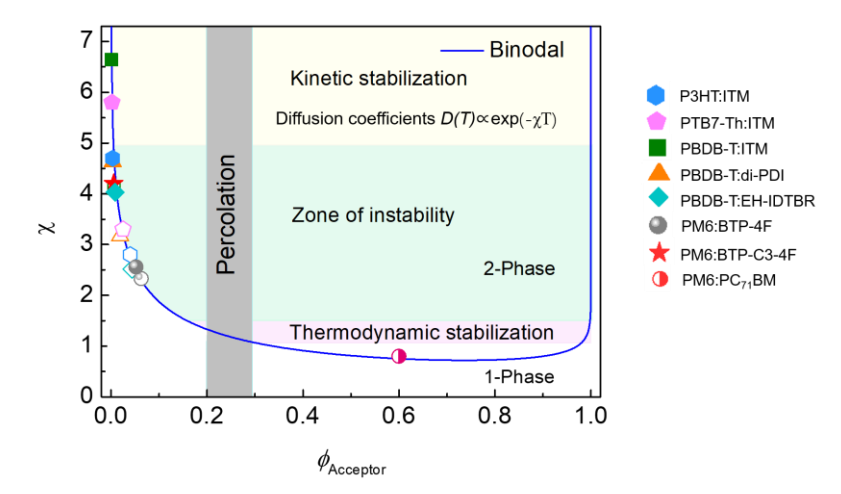


**Figure 1**. Motivational illustrations of the  $\chi-\phi$  phase diagram with  $\chi(RT)$  (filled symbols) and  $\chi(85^{\circ}C)$  (Open symbols). Data for all but PM6: BTP-C3-4F (N3) and PM6:BTP-4F is an extrapolation from high temperature ToF-SIMS data<sup>35</sup>. PM6: BTP-C3-4F and PM6:BTP-4F are using a RT solvent vapor annealing (SVA) protocol. Note that a  $\chi$  of approx. 1.3 leads to mixed domains that have a composition near the percolation threshold and the morphology can be considered to be "thermodynamically" stabilized as the kinetics of coarsening of the domains size is extremely slow. A  $\chi>5$  leads to strong kinetic stabilization as the diffusion coefficients  $D(T) \propto \exp(-\chi_H T)$ , where  $\chi=\chi_S+\chi_H$  (i.e.  $\chi$  is composed of an entropic and enthalpic contribution).<sup>35</sup> Except for some exceptions,  $\chi \propto \chi_H$  and  $D(T) \propto \exp(-\chi T)$ . The conceptual boundary to kinetic stabilization is gradual and not as sharp as indicated. Morphologies of PM6:BTP-4F and PM6: BTP-C3-4F are neither thermodynamically nor sufficiently kinetically stabilized against over-purification and possibly crystallization, particularly at higher temperatures where diffusion proceeds more readily.

The general observation that ternary or quaternary devices can, under certain conditions, maintain charge percolation and improve stability has been rationalized recently by showing that the ternary component needs to have a miscibility in the donor polymer above the percolation threshold and low miscibility in the second acceptor to assure that the third component is partitioned into and residing in the mixed, polymer-rich domains, assuring electron transport across the mixed domains<sup>28</sup>. A ternary component that mixes too strongly with the acceptor would likely be immiscible with the polymer and would not prevent the loss of percolation.





This background and recent advances raise interesting questions: i) What is the  $T_g$  and thus predicted relative stability of the various BTP NFA analogs? and ii) if they are all intrinsically unstable in binary devices due to high diffusion coefficients as inferred from their Tg, can they be stabilized with the addition of PC71BM, the most common second acceptor in ternary devices and by what mechanism? We address these two interrelated questions by determining the thermal transition temperature indicative of  $T_g$  of BTP-4F and its BTP-4F-C12, BTP-4F-DT (DTY6), BTP-eC7, BTP-eC9, BTP-eC11, and BTP-C3-4F analogs to develop a structure-  $T_{\rm g}$  framework that informs expected relative stability. We are particularly interested in the combination of performance and stability, and thus investigate PM6: BTP-C3-4F (the highest performing of the three highest  $T_g$  systems) in detail and benchmark stability against PM6:BTP-4F. We also show that PC<sub>71</sub>BM has a miscibility above the percolation threshold in PM6 and should thus be able to stabilize binary solar cells. Unfortunately, the stability of PM6: BTP-C3-4F:PC71BM is still insufficient and the development of unfavorable vertical gradients is not suppressed as the PCBM does not prevent BTP-C3-4F diffusion. The development of BTP analogs with a higher  $T_g$  and lower diffusion coefficient is highly desirable to achieve intrinsically improved morphological stability, that is the prevention of over-purification of the mixed domains, suppression of crystallization, and suppression of an unfavorable vertical gradient. Based on the observed correlation of chemical structure and  $T_g$ , achieving the stability level of ITIC/IT-M ( $T_g = \sim 160$  °C) or IEICO-4F ( $T_g = \sim 190$  °C)<sup>32-33, 35</sup> family of NFAs is completely out of reach for acceptors with a BTP core. Moderate gains could be achieved with slightly shorter side-chains, at the cost of further reduced performance, as the fluorinated molecules have already been optimized with the BTP-C3-4F analog (over BTP-4F) and the chlorinated molecules with BTP-eC9 (over BTP-eC7). In the absence of an eventual ternary or quaternary strategy that prevents diffusion of the BTP-based NFAs, it is highly likely that a new family of NFAs or a different donor polymer needs to be discovered or developed to achieve high performance and high stability at the same time.

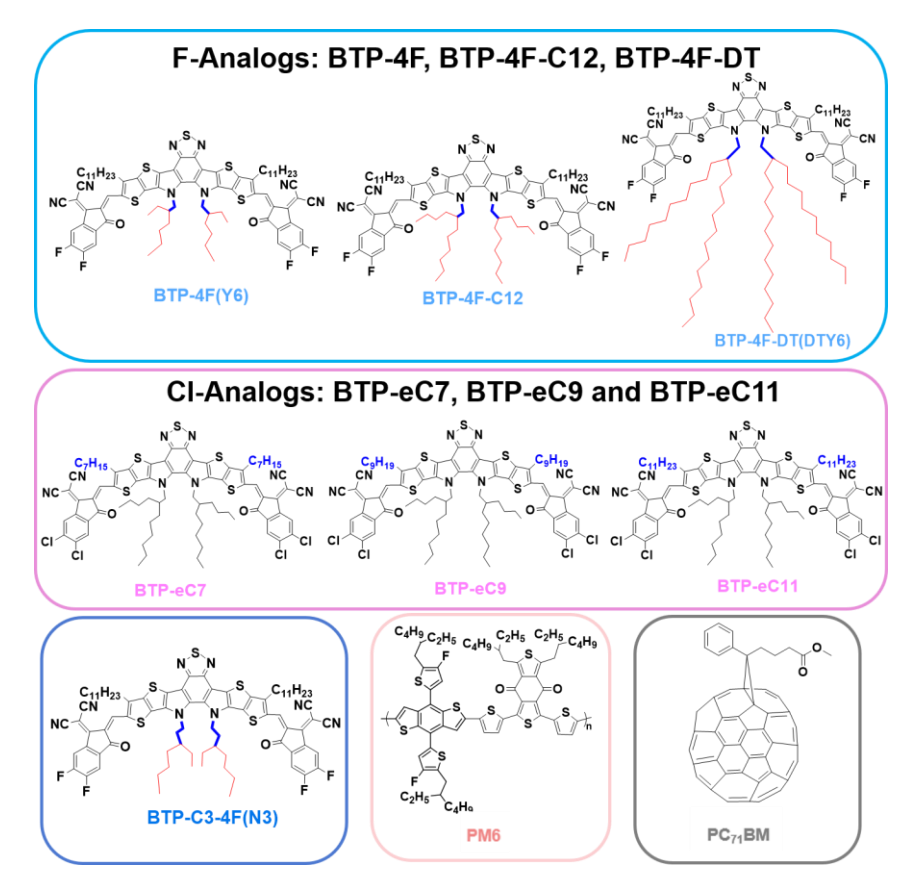


Figure 2. The chemical structures of the materials used in the study.

# **RESULTS**

#### **Basic Thermodynamic Properties**

The chemical structures of the materials used in the current study are depicted in **Figure 2**, We note that the seven BTP analogs consist of two homologous series (fluorinated BTP-4F, BTP-4F-C12, BTP-4F-DT and chlorinated BTP-eC7, BTP-eC9, BTP-eC11) and BTP-C3-4F. The UV-vis deviation metric results (see **Figure S1** for raw data and methods) for the seven analogs studied are displayed in **Figure 3**. Thermal transition temperature can be readily observed with the following results for the two homologous series: for BTP-4F ( $102 \pm 1 \,^{\circ}$ C), BTP-4F-C12 ( $78 \pm 1 \,^{\circ}$ C), BTP-4F-DT ( $50 \pm 1 \,^{\circ}$ C), BTP-eC7 ( $85 \pm 1 \,^{\circ}$ C), BTP-eC9 ( $75 \pm 1 \,^{\circ}$ C), BTP-eC11 ( $69 \pm 1 \,^{\circ}$ C) and BTP-C3-4F ( $82 \pm 1 \,^{\circ}$ C), respectively. According to the Ade-O'Connor-Ghasemi stability framework<sup>35</sup>, BTP-4F should possess the smallest diffusion coefficients and BTP-4F-DT the largest and the related inverse relative ranking for kinetic stabilization.

Joule Cell<sup>P</sup>ress

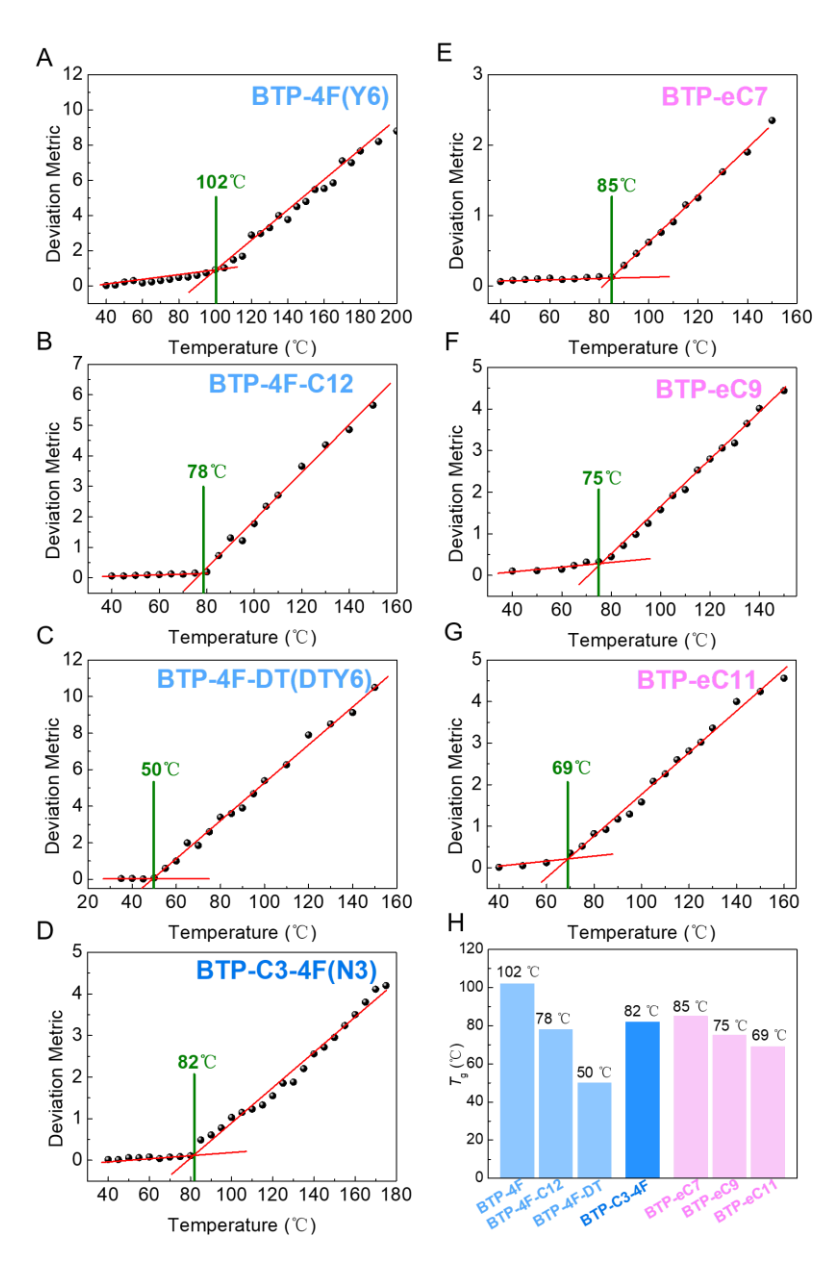


**Figure 3**. UV-vis deviation metric results for the (A-D) fluorinated-analogs, (E-G) chlorinated-analogs and (H) the summary of the  $T_g$  of the seven BTP-analogs.

Exposure to heat accelerates changes in nanostructure through enhanced diffusion of the blend components, which accelerates demixing and crystallization. For this reason, the bulk-heterojunction (BHJ) blend nanostructure must be able to withstand repeated heating without significant changes. As per the international standards, in order to certify a solar cell as stable, the device must be able to withstand thermal cycling between -40 and 85 °C<sup>40</sup>. Ideally, the miscibility and diffusion coefficients are known over the full temperature range. This is very



difficult though and often high-temperature measurements are used that are extrapolated into the operating ranges of the devices. One such method uses bilayer interfusion measurements that can not only provide diffusion coefficients, but also the equilibrium composition that corresponds to the binodal as a function of temperature. These measurements are often constrained to be made at T>120 ° C, but when several measurements are available, they can be used to extrapolate into the -40 to 85 °C range. Here, for simplicity, we utilize time-of-flight secondary ion mass spectrometry (ToF-SIMS) measurements on bilayers solvent annealed at RT to check the miscibility of BTP-4F, BTP-C3-4F, and PC71BM in PM6 (see Figure S2). The results, converted to χ, are included in Figure 1 and confirm that BTP-4F and BTP-C3-4F are highly immiscible in PM6, whereas PC71BM is highly miscible. PM6:BTP-4F and PM6: BTP-C3-4F are is expected to be unstable. PCBM should be able to stabilize the performance by providing electron percolation in the PM6 matrix.

## Rationale of Systems Investigated as Devices

Our studies have two primary goals: 1) Reveal structure-thermal property relations amongst BTP analogs in order to derive a framework that can disentangle the contributions of the different side-chains and the core to the Tg, and 2) understand the mechanism of success or failure of stabilizing a high efficiency system with PCBM. To connect the two goals, we characterize a limited set of binary and ternary devices. Since BTP-C3-4F exhibits improved properties and performance over BTP-4F due to more favorable domain size and more dominant face-on orientation of the  $\pi$ - $\pi$  stacking <sup>13</sup>, yet is amongst the three highest  $T_g$  materials, we investigated PM6: BTP-C3-4F binary and PM6: BTP-C3-4F:PC71BM ternary in the inverted geometry in detail, including their morphology and device physics. We also reason that the impact of PC<sub>71</sub>BM stabilization and reason for failure might be more quickly apparent if not the highest  $T_g$  system would be chosen. We explored the device stability by fabricating and characterizing the solar cells by using an inverted structure of ITO/ZnO/active layer/MoO<sub>3</sub>/Al. The general device processing conditions were similar to our previous work and similar efforts11. For fabrication and other experimental and protocol details, see EXPERIMENTAL PROCEDURES. The BTP-C3-4F-based device performance and stability are benchmarked against BTP-4F-based devices, fully cognizant that a direct comparison of diffusion-caused device stability is complicated because the device performance is impacted by FF, J<sub>SC</sub> and V<sub>OC</sub>, which in turn are dependent on several morphology related parameters (size, purity, connectivity, aggregation, molecular orientation, vertical gradients)



and by the inability to quench to precisely the same morphology or to a defined composition in relation to the percolation threshold<sup>32</sup>. Our goal is not to untangle this complexity, but to understand the basic structure-thermodynamic property relations of BTP analog devices, and the thermodynamic mechanism for improved performance with PCBM and the residual failure pathway in the ternary devices.

#### Storage Stability of the Binary and Ternary Solar Cells

As mentioned above, we are interested in the combination of performance and stability, and to investigate PM6: BTP-C3-4F in detail and to benchmark stability against PM6:BTP-4F, we first studied and compared the stability of BTP-C3-4F and BTP-4F based binary and ternary devices. The binary BTP-4F and BTP-C3-4F based systems exhibit pronounced performance degradation even at RT after storing in the dark an N2-filled glovebox. The ZnO interlayer would cause additional photo-degradation, but the devices were deliberately stored in the dark to investigate the impact of morphological changes, which can be accelerated or slowed down by heating or cooling, respectively<sup>41,42</sup>. Consequently, in addition to the RT studies, we explored the thermal stability by continuous aging at 80 °C, which is below the  $T_g$  of BTP-C3-4F but close to the upper limit of 85 °C in the rigorous stability cycling test, as well as aging at 100 °C and 120 °C. We will refer to the samples stored in the N<sub>2</sub>-filled glovebox at RT as "RT" whereas the samples stored in the N2-filled glovebox by continuous aging at 80 °C as "T80", and continuous aging at 100 °C, as "T100". The devices were only exposed to light during the short occasional measurements. The device performance parameters are summarized in Table S1 and S2. Figure 4 displays the stability of the RT and T80 binary and ternary devices. The stability data were collected from four devices measured under the same aging conditions. The incorporation of the PC71BM can suppress the degradation of the devices and improve the performance of the fresh devices at the same time. As shown in Figures 4A and 4D, after the 600 hours storage, the RT PM6: BTP-C3-4F:PC71BM ternary devices maintain 94% of the initial PCE compared with 80% of the initial PCE of the binary devices. For the T80 devices, the stability can improve from 66% of the initial PCE of the binary devices to 84% of the initial PCE of the ternary devices. Whereas, the RT PM6:BTP-4F:PC71BM ternary devices maintain 96% of initial PCE compared to 91% of the initial PCE of the PM6:BTP-4F binary devices. For the T80 devices, the stability can improve from 71% of the initial PCE of the binary devices to 86% of the initial PCE of the ternary devices. We further analyzed the extrapolated  $T_{80}$  (80% of the initial PCE) lifetime as shown in Figure 4B and 4C, the results for BTP-C3-4F based devices show an improved extrapolated  $T_{80}$  lifetime of up to 9950 hours and 3090 hours for the



ternary, compared to the poor  $T_{80}$  lifetime of 715 hours and 175 hours for the binary. Meanwhile, for BTP-4F based devices, the  $T_{80}$  lifetime can boost to 12200 hours and 4778 hours for the ternary, compared to a poorer  $T_{80}$  lifetime of 2000 hours and 230 hours for the binary (see **Figure 4E** and **4F**), which means the BTP-4F based devices have better stability than the BTP-C3-4F based devices. This agrees well with our previous explanations and inferences from the  $T_g$ . Finally, we compare the thermal stability at continuous 100 °C/120 °C with the thermal stability at continuous 80 °C and calculated the  $T_{80}$  lifetime, which are shown in **Figure S3-Figure S5**. For the BTP-C3-4F based T100 devices, both the binary and ternary showed worse stability while for the BTP-4F based T100 devices, both the binary and ternary showed similar stability with the T80 devices. This confirms that the NFA  $T_g$  is a critical parameter for the thermal stability of OSCs as the annealing temperature 100 °C is higher than the  $T_g$  of BTP-C3-4F, but lower than the  $T_g$  of BTP-4F. Finally, we choose BTP-C3-4F based devices for the systematic discussion presented below that includes fresh, RT and T80 conditions due to the higher initial performance of the BTP-C3-4F-based device and slightly larger degradation to understand the mechanism.

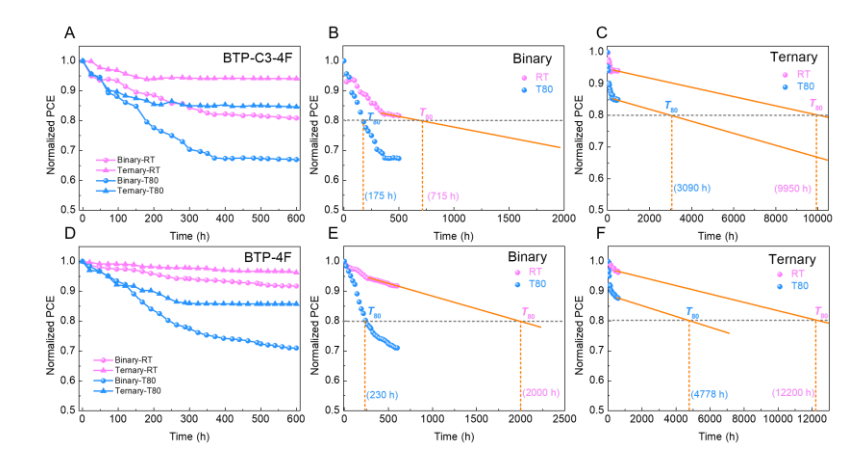


**Figure 4.** Device stability at the RT and T80 conditions of (A) BTP-C3-4F and (D) BTP -4F based binary and ternary solar cells and the  $T_{80}$  lifetime analysis of (B) BTP-C3-4F and (E) BTP -4F based binary and (C) BTP-C3-4F and (F) BTP-4F based ternary devices.

# Morphological Stability of the Binary and Ternary Solar Cells

The study of morphological stability is directly related to the initial BHJ nanostructure and its evolution. Herein, we investigate the coherence length (CL) and mesoscale structure of the blend films by performing grazing incidence wide-angle X-ray scattering (GIWAXS) at Advanced Light Source<sup>43-46</sup>. The in-plane (IP) and out-of-plane (OOP) 1D profiles and 2D



images of pristine and blend films are shown in **Figures S6-S8**. PM6 pristine fresh and aged films showed  $\pi$ - $\pi$  stacking peak at the q value of 1.72 Å<sup>-1</sup> in the OOP direction and showed no obvious changes with aging in both the IP and OOP directions. Meanwhile, for the fresh and RT/T80 acceptor (BTP-C3-4F and BTP-C3-4F:PC71BM), the CL of BTP-C3-4F increases significantly in the aged films while the aged films of BTP-C3-4F: PC71BM shows comparatively small changes (see **Table S3**), which indicates that the PC71BM may work as a stabilizer by preventing aggregation and crystallization. A similar trend is observed for the binary and ternary blend films, namely, the CL of the aged ternary films show negligible changes while a pronounced CL change was observed for the binary films. (see **Table S4**).

# **Charge Carrier Recombination and Lifetime**

In general, the FF of highly efficient OSCs is directly reflective of the charge recombination. To gain deeper insight into the extent of charge recombination changes due to the aging of the binary and ternary devices, charge carrier lifetime ( $\tau$ ) and charge carrier density (n) were acquired using the transient photo-voltage (TPV) and charge extraction (CE) techniques, and the results are shown in **Figure 5A** and **5B**. By using the equation  $\tau = \tau_0 (n_0/n)^{\lambda}$ , where  $\tau_0$  and  $n_0$  are constants and  $\lambda$  is the so-called recombination exponent, a recombination order  $R = \lambda + 1$  equal to 2 indicates almost perfect bimolecular recombination. On the other hand, a recombination order higher than two is attributed to the effect of trapping and release in energetic traps, as well as morphological traps<sup>47,48</sup>. The calculated R for the fresh and RT/T80 aged devices are shown in the inset of Figure 5A and 5B, respectively. Fresh binary and ternary devices exhibit an almost ideal bimolecular recombination (R=2.06 and 2.02). However, after aging, the recombination order of the binary devices increases to 2.38 for the RT stored condition and 2.76 for the T80 stored condition. In contrast, the value for the ternary devices showed only a slight increase to 2.09 for the RT stored condition and 2.16 for the T80 stored condition, indicating that the ternary can effectively reduce the trap-related recombination or morphological defects, which is directly correlated with the degradation of the performance in the binary.



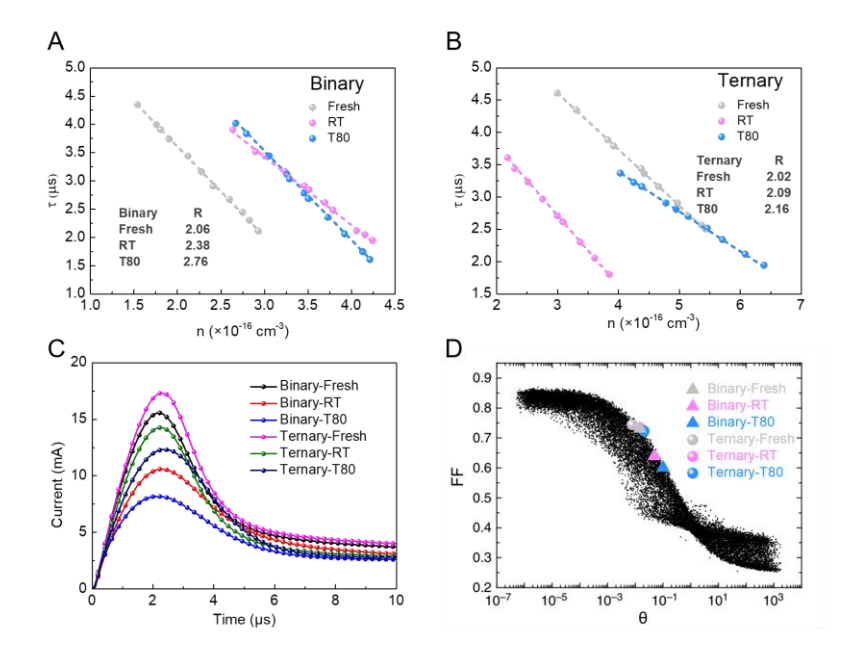


Figure 5. Charge carrier lifetime  $\tau$ , obtained from TPV, versus charge density n, calculated from CE measurement for (A) binary and (B) ternary based OSCs; (C) The Photo-CELIV of fresh and aged binary and ternary based OSCs; (D) FF as a function of  $\theta$  (Figure of merit for competition between charge carrier extraction and recombination) calculated according to the literature and the simulated data is from the literature<sup>48</sup>.

To gain more insight into the charge transport behavior in the devices, we investigated the charge carrier mobility by employing the photo-induced charge carrier extraction by linearly increasing voltage (photo-CELIV) measurements on fresh and aged devices in both binary and ternary systems. As shown in **Figure 5C** and **Table S5**, it is revealed that the binary devices showed lower mobilities and dispersive transport after aging, which is attributed to traps and this is consistent with the increasing recombination exponent discussed earlier. In contrast, the ternary devices show an insignificant change in carrier mobility. Bartesaghi et al.<sup>49</sup> have reported a dimensionless parameter  $\theta$  that quantifies the ratio of charge recombination and extraction rates. In general,  $\theta$  can reflect the effect of charge-carrier mobilities, recombination rate, thickness, light intensity as well as internal voltage. Herein, we calculated the parameter  $\theta$  of the fresh and aged devices to understand its corrections with FF. As shown in **Figure 5D**,  $\theta$  values obtained from the aged and fresh samples show a typical trend that follows the reported simulated data, and the changes observed in FF can be attributed to the varying charge carrier mobility and recombination processes discussed earlier. To further explore the role of charge





mobility, the space charge limited current (SCLC) method was employed, as shown in **Figure S9** and **Table S6**, the results reveal a strong reduction in mobility in binary devices as a result of aging, while the ternary devices show smaller changes. This trend is consistent with the mobility of the fastest carrier measured with photo-CELIV (see Figure **Table S5**), which indicated the FF degradation originates most probably from the decreased charge mobility.

#### Depth profiles of the fresh and aged devices

To better understand and explain the observed difference in device stability of the binary and ternary systems and to investigate why the ternary devices are not completely stabilized as thermodynamic considerations of the bulk morphology would imply, we utilized ToF-SIMS to provide the depth profiles across the whole thickness of both the fresh and aged devices. We investigated at locations next to the Al electrodes with the MoO3 transport layer as the top surface (no sacrificial layer for ToF-SIMS characterization was used). By tracking the distribution of elements or unique fragments across the depth of the active films, we can obtain valuable information regarding the homogeneity of the donor and acceptor across the active layer. This specifically allows us to infer if there is a thermodynamic interfacial driving force (interfacial energy) for the development of a gradient and if the interlayers are stable. Figure 6 displays some characteristic elements and ions as a function of depth from fresh, RT and T80 binary and ternary blends. Most crucially, we utilize the CN signal to uniquely follow the distribution of BTP-C3-4F. The RT/T80 binaries exhibit a pronounced vertical gradient, with a concentration of BTP-C3-4F about a factor of two higher at the anode than at the cathode for T80 devices. In contrast, the depth distribution of CN- fragment indicates only a slight vertical segregation across the active layer in the ternary system. Thus, the intensity of CN is higher near the MoO<sub>3</sub> anode interface in aged films, which indicates the BTP-C3-4F acceptor is prone to accumulate near the MoO3 anode interface, leading to a reduction in FF and most likely the reduction in  $V_{\rm OC}$  as well, the two parameters degrading the most. Importantly, the as-cast devices have a more favorable BTP-C3-4F vertical distribution profile, and aging induces unfavorable profiles in binaries and ternaries. Though both the aged binary and ternary systems developed an unfavorable vertical gradient, the ternary had a smaller gradient and smaller BTP-C3-4F concentration near the anode interface. This is in agreement with the smaller degradation in FF,  $V_{\rm OC}$ , and PCE in the ternary system.



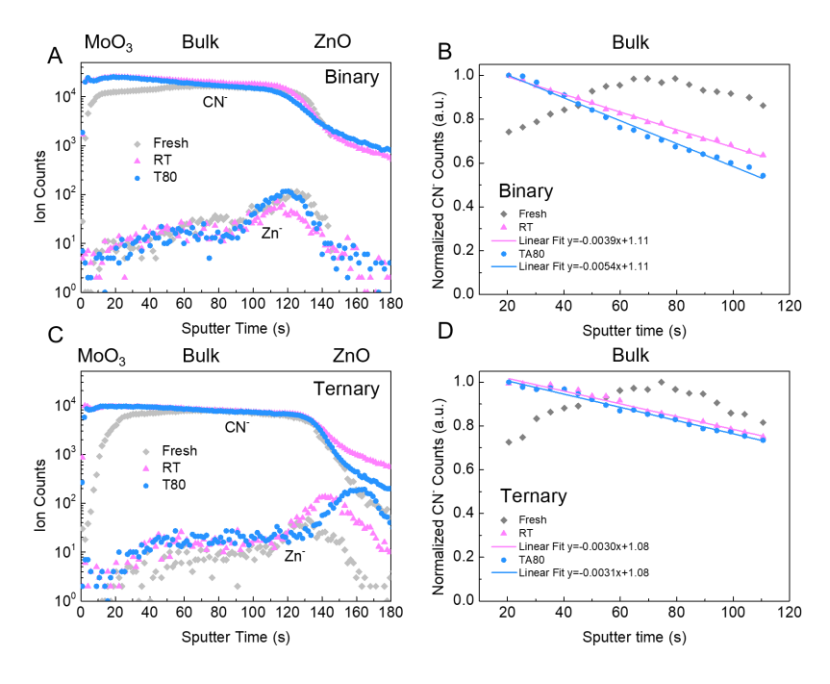


**Figure 6.** Depth profiles of the (A) binary and (C) ternary before and after degradation. Extracted data of the binary (B) and (D) ternary of the CN<sup>-</sup> signal that tracks BTP-C3-4F (and Zn<sup>-</sup> for ZnO) after degradation. We note that it is difficult to rigorously translate sputtering time into depth. We have just only loosely indicated that the MoO<sub>3</sub> layer is on the left and the ZnO layer on the right of the concentration traces, with the ZnO interfaces reached at slightly different times in the different samples.

To understand these differences in gradients, we measured the BTP-C3-4F thermal transition temperature of the binary (82 ±1 °C) and ternary (82 ±1 °C) in order to see if the reduction in gradient for the ternaries is a kinetic or thermodynamic effect. We could not observe any difference in the thermal transition in mixtures that use the device composition ratios of weight ratio of PM6: BTP-C3-4F: PC71BM = 1:1:1 (See **Figure S10**). To check the impact on the thermal transitions when PC71BM is more likely mixed with the BTP-C3-4F, we characterized the 1:1 BTP-C3-4F:PC71BM acceptor binary and found that the BTP-C3-4F thermal transition temperature increases to 89 ±1 °C (See **Figure S11**). In this case, the BTP-C3-4F and PC71BM form BTP-C3-4F and PCBM-rich mixed domains limited by the binodal composition. The higher  $T_g$  of PC71BM (~160 °C) (See **Figure S12**) raises the transition temperature in the BTP-C3-4F-rich mixed domains. We are unable to observe  $T_g$  of the PC71BM-rich domains by the UV-Vis method, as its absorption spectrum barely changes even in pure PC71BM when annealed (**Figure S13**). An estimate based on the change in  $T_g$  and using



the Fox equation yields a concentration of  $\sim$ 11% of PC<sub>71</sub>BM in the BTP-C3-4F-rich domains, indicating that PCBM is relatively immiscible with BTP-C3-4F. Given that observed changes in  $T_{\rm g}$  for the 1:1 BTP-C3-4F:PC<sub>71</sub>BM acceptor binary, the observation that the thermal transition temperature remains at 82 °C for the ternaries is significant. We conclude, supported by the high miscibility of PC<sub>71</sub>BM with PM6 (60%) but much lower miscibility with BTP-C3-4F ( $\sim$ 11%), that PC<sub>71</sub>BM is only partially mixing within the BTP-C3-4F in the ternary but instead resides primarily in the disordered volume fraction of the PM6. Reduction of the vertical segregation of BTP-C3-4F in the ternaries is thus not a kinetic suppression by lowering BTP-C3-4F diffusion coefficients, but a modification of one or both interfaces by PC<sub>71</sub>BM that reduces the driving force for BTP-C3-4F stratification. While it is highly desirable to also trace the PC<sub>71</sub>BM vertical gradient, we were unsuccessful to do so.

#### DISCUSSION

#### Thermodynamics and morphology relations to performance

We show here that all observations about the device morphology stability can be consistently described by thermodynamic characteristics. The PM6:BTP-C3-4F and PM6:BTP-4F binary systems exhibit strong morphology degradation, which is directly related to the phase diagram. With a  $\chi=4.2$  and 2.6 at RT, respectively, which corresponds to a polymer-rich mixed phase with 0.58 vol % BTP-C3-4F and 8.5 vol % BTP-4F in the polymer, the binodal concentration of the BTP-C3-4F is well below the percolation threshold of ~25%. There is, thus, a significant thermodynamic driving force for the mixed, polymer-rich domains to overpurity, yet, the miscibility is not low enough to lead to kinetic stabilization with low diffusion coefficients that are associated with systems that have  $\chi > 5$  and thus high activation energy for diffusion. The PM6: BTP-C3-4F and PM:BTP-4F are in the zone of instability in the phase diagram (see **Figure 1**).

The morphological stability of these mixed domains, or lack thereof, can be predicted from  $\chi$  and by the  $T_g$  of the NFA as a proxy parameter. According to the Ade-O'Connor-Ghasemi framework <sup>32,35</sup>, an NFA with a high  $T_g$  (e.g., ITIC/ITM or IEICO-4F) has a low diffusion coefficient and can suppress crystallization and demixing, leading to relatively stable operation. However, the  $T_g$ s of BTP-4F and its BTP-4F-C12, BTP-4F-DT, BTP-eC7, BTP-eC9, BTP-eC11 and BTP-C3-4F analogs are 102 °C, 78 °C, 50 °C, 85 °C, 75 °C, 69 °C and 82 °C, respectively, much lower than the  $T_g$ s of the ITIC/ITM or IEICO-4F family of NFAs. Such a low  $T_g$  leads to a relatively low  $\chi$ , with a high diffusion coefficient, which directly leads to the



degradation of the PM6:BTP-C3-4F and PM6:BTP-4F binary devices through overpurification of the mixed domains and, importantly, also the development of an unfavorable vertical gradient with the accumulation of BTP-C3-4F near the anode. The ability for the BTP-C3-4F to diffuse in the binary and ternary devices was directly observable in the evolution of the vertical distribution during aging. The ability to diffuse will eventually lead to crystallization, an additional significant mechanism for degradation<sup>32,34</sup>.

The stabilization by PC<sub>71</sub>BM is directly related to its measured high miscibility in PM6 and its inferred low miscibility in BTP-C3-4F. This results in maintaining a PC<sub>71</sub>BM concentration in the polymer-rich mixed domains that are above the percolation threshold even at low overall PC<sub>71</sub>BM loading and thus being able to sustain charge separation and electron transport in the mixed domains, and reduce the likelihood of trap assisted recombination by reducing the number of islands that act as traps and a lowering of the mobility. Additionally, the PC<sub>71</sub>BM also reduced the development of an unfavorable vertical gradient<sup>50</sup>. As a result, the ternary showed an improved extrapolated T<sub>80</sub> lifetime compared to the binary. Though PC<sub>71</sub>BM should and does stabilize the mixed, polymer-rich domains, it is not enough as it does not mix with BTP-C3-4F and is not acting as a diffusion stabilizer. The stability of PM6: BTP-C3-4F:PC<sub>71</sub>BM, even PM6:BTP-4F:PC<sub>71</sub>BM is still insufficient for commercialization as the ternary devices still exhibit vertical diffusion of BTP-C3-4F that leads to an unfavorable gradient. The development of a BTP analog with a higher T<sub>g</sub> is highly desirable to improve stability.

# Molecular design – $T_g$ framework

Lastly, we discuss the impact of molecular design on  $T_{\rm g}$  to explore if a stable BTP analog can be created. Reimschuessel<sup>51</sup> reported that the characteristics of  $T_{\rm g}$  may be indicative of the various interactions of the backbone and side chains. An increase in the length of the side chain will result in a larger free volume, a reduced packing density, and thus a reduced steric hindrance to segmental mobility. This kind of internal plasticization is characterized by a lower activation energy of the segmental motion and a lower glass transition temperature. Here, we compared the seven BTP analogs In this case, the  $T_{\rm g}$  exhibits a general decline as a function of the alkyl side chain length, as shown in **Figure S14**. Our results agree well with the trends observed in the previous studies of poly (3-alkyl-thiophene) (P3ATs), poly N-(n-alkyl-maleimides) and poly (styrene-co-alkyl-maleimide) <sup>51-55</sup>: the smaller the total length of all sidechains (in relation to given backbone), the higher the  $T_{\rm g}$ .



How high could the  $T_{\rm g}$  of BTP-4F analogs be pushed with a modified molecular design in order to achieve improved stability? For an empirically designed high-efficiency material, we usually consider the effects of solubility, energy level, absorption, and morphology, etc. Since shorter side chains would negatively affect solubility, processability and likely performance, there is a limit to how short the chains can be made. Since we have only investigated seven BTP analogs (four F-analogs BTP-4F, BTP-4F-C12, BTP-4F-DT, BTP-C3-4F and three Clanalogs BTP-eC7, BTP-eC9 and BTP-eC11), we utilize the prior results on P3ATs, poly N-(nalkyl-maleimides), and poly (styrene-co-alkyl-maleimide) referenced above to guide an estimate of the side-chain length needed to reach a T<sub>g</sub> of ~160 °C, a minimum transition temperature that is needed for high morphological stability. We compare and reanalyze these data by plotting T<sub>g</sub> against φ (the side-chain mass fraction) (see Figure 7 and S15). Here, we disregard the  $T_g$  data points for the higher  $\varphi$  values of the poly N-(n-alkyl-maleimides) as the longer side-chains lead to the crystallization or regions of crystalline order. This results in an increase in the  $T_{\rm g}$  of the polymer or signification deviation from the linearly reducing  $T_{\rm g}$  51,53. Thus, only data with sufficiently short side-chains i.e. below the critical side-chain length should be used for the analysis of the linear region of the  $T_g - \varphi$  relation. A similar behavior is also observed in the case of P3ATs, where P3DDT exhibits side-chain crystallization (C-atom = 12) resulting in a higher  $T_g$  of P3DDT compared to P3DT(see **Figure 7**)<sup>54</sup>. Utilizing these considerations, excellent linear relations between  $T_g$  and  $\phi$  are observed with Pearson correlation coefficients of > 0.98 in all three cases so analyzed. This linearity indicates that the combined  $T_g$  of the polymers is simply the weighted average of the intrinsic  $T_g$ s of the backbone and the side-chains, a conclusion supported by the Gordon-Taylor equation<sup>56</sup>. Furthermore, if we extrapolate the linear fits, we observe  $T_g(1) = -100$  to -60 °C (173 K to 213 K). As  $\varphi = 1$ corresponds to the limit of infinite side-chain length, the expected  $T_{\rm g}$  can be compared to the related model systems. Here, we use polyethylene as a reference and note that the  $T_{g\beta}$  transition of linear low density polyethylene (LLDPE) is at 237 K (= - 36 °C)<sup>57</sup>. This agrees closely with the analysis here. We attribute the difference to be due to the departure from linearity by the crystallization in LLDPE as discussed above.



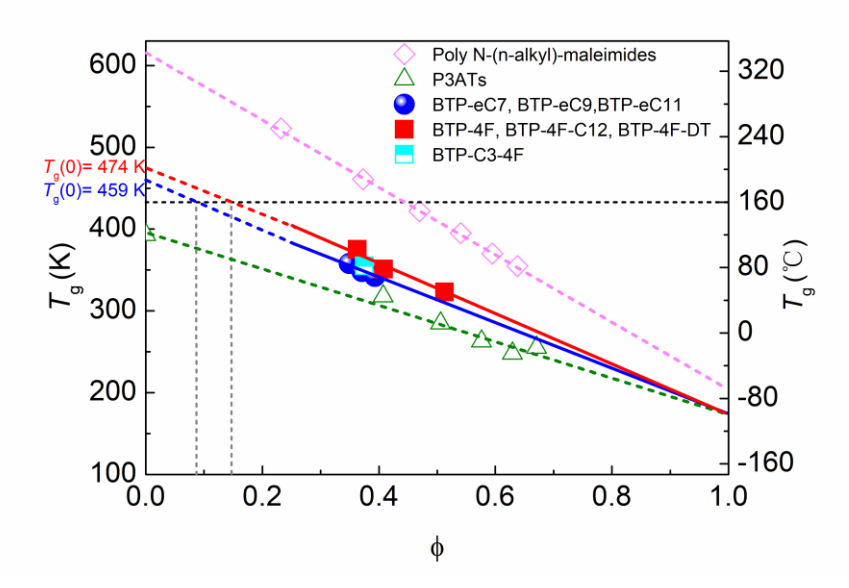


**Figure 7.** Empirical relationship and linear fits between the  $T_g$  and the side chain mass fraction  $\varphi$  of BTP-4F, BTP-4F-C12, BTP-4F-DT, BTP-C3-4F, BTP-eC7, BTP-eC9 and BTP-eC11 and poly N-(n-alkyl-maleimides), and P3ATs from select previous studies. The database and structures are presented in the Supplemental Information 51-53.

In striking similarity to the three homologous reference materials, our results for the two homologous BTP analogs series investigated yield linear fits with very similar slopes and asymptotic  $T_g$  (1). Firstly, BTP-eC7, BTP-eC9 and BTP-eC11, which differ only in the length of the outer unbranched side-chains with 7, 9 and 11 carbon atoms, should and does follow the behavior of the homologous reference materials. A linear fit (the blue line) through the BTPeC7, BTP-eC9 and BTP-eC11 data yields a  $T_g(1) = 175$  K. A linear fit (the red line) through the BTP-4F, BTP-4F-C12 and BTP-4F-DT data yields a  $T_g(1) = 173$ K. Both are close to each other and close to  $T_g$  (1) of the P3ATs, validating the general model's utility. The slightly different slopes of the two analog series indicate that the outer and inner(bay) side-chains contribute slightly differently to the  $T_g$  of the molecule. Consequently the extrapolation to a target Tg of 160 °C (the dashed black line), a temperature we deem is needed for long term stability<sup>35</sup>, is complex, as the linear fit becomes unphysical at  $\varphi = 0.250$  for the outer sidechains (as only the inner chains contribute how to  $\varphi$ ) and  $\varphi = 0.253$  for the inner extrapolations (the only contributing side-chain mass fraction is from the outer side-chains). At these points, we have to switch to the slope (dashed portion) that corresponds to the complementary side-chains. In this way, we estimate  $\varphi = 0.089$  for the F-analogs and a  $\varphi = 0.147$ . The corresponding short



side-chains needed to reach a  $T_g$  of 160 °C would make the BTP molecules unusable for high performance (see discussion below).

The two homologous series can also provide insight to untangle the impact of halogenation. Going from BTP-4F to BTP-eC11, the bay-position sidechains have the same branching position but both branches got longer by two alkane units. We can get the  $T_{\rm g}$  of 78 °C (BTP-4F-C12), which have the same alkyl side chain but different halogenation with BTP-eC11 (69 °C), which means the use of Cl is leading to a lower  $T_{\rm g}$  than F. Additionally, the two data sets for the F and Cl homologous series are clearly separated and extrapolation, accounting for the differences in outer and inner sidechains, to  $T_{\rm g}$  (0) yields 474 and 459 K, respectively.  $T_{\rm g}$  (0) should be the  $T_{\rm g}$  of just the core and the differences observed are due to the different halogenation. The methodology and analysis protocols presented opens up an avenue to disentangle structure –  $T_{\rm g}$  relations even in very complex molecules such as BTP-based NFAs and likely other NFAs as well.

Due to the different branching points for BTP-C3-4F from BTP-4F, BTP-4F-C12, and BTP-4F-DT, we did not include it in the linear fit of the latter molecules discussed above. If included, the fits do not change much (see **Figure S15**), consistent with the visual clustering of the data in **Figure 7**. This would indicate that the branching point has only a minor impact on the  $T_g$ .

In the case of the BTP analogs and most likely in general, a most critical and unresolved molecular design conundrum emerges on how to simultaneously achieve high processibility, performance and intrinsic stability. This conundrum and predicament can already be observed within the set of seven BTP-4F analogs we have investigated. BTP-4F has worse performance than BTP-C3-4F for the fluorinated analogs and BTP-eC7 performs significantly worse than BTP-eC9 (see **Table S10**). The side-chains have already been optimized for performance and improved stability (as implied by extrapolation of the  $T_g$  measurements) would be at the cost of reduced performance.

# CONCLUSIONS

Considering the totality of these results, a coherent view emerges that connects thermodynamics, kinetics, thermal properties, stability with molecular design. We addressed our two primary objectives in relation to the three morphological degradation pathways as follows: 1) We determined the thermal transition temperatures of seven BTP-analogs to infer relative stability and developed a methodology and analysis protocols that allow disentangling



structure –  $T_g$  relations even in very complex molecules such as BTP-based NFAs. The slightly different impact of the outer and inner (bay) sides on the Tg could be clearly delineated, Similarly, the contribution of the core to the  $T_g$  could be inferred and the differences between chlorination and fluorination determined. 2) We delineated the thermodynamic mechanism by which PC71BM stabilizes the devices, but fails to reduce the BTP-C3-4F diffusion. PC71BM is highly miscible with PM6, but only marginally miscible (11%) with BTP-C3-4F. It is thus preferentially located in the polymer-rich, disordered regions of the donor, able to provide charge percolation. As a result, the ternary showed a significantly improved extrapolated T<sub>80</sub> lifetime of up to 9950 hours compared to the poor T<sub>80</sub> lifetime of 715 hours of the binary. Although PC<sub>71</sub>BM can maintain charge transport in the mixed domains, it cannot completely prevent detrimental vertical diffusion of BTP-C3-4F that leads to the development of an unfavorable BTP-C3-4F gradient that leads to increased trap-assisted charge recombination. The high diffusion observed also implies that crystallization is likely a relevant degradation pathway. The inability of the PC<sub>71</sub>BM to prevent diffusion is directly related to its ability to maintain percolation by having a miscibility above the percolation threshold. Any thigh high T<sub>g</sub> acceptor that prevents BTP-C3-4F diffusion would have to have high miscibility with BTP-C3-4F and thus likely a low miscibility with PM6 similar to that of BTP-C3-4F. Consequently, it would not mix enough to maintain percolation unless kinetically trapped. For these thermodynamic reasons it is unlikely that a single component additive can maintain percolation and reduce BTP-C3-4F diffusion. A single additive that would lower diffusion everywhere in the device would have to have a high  $T_g$  and partition in the same proportion in the various domains at the BTP-C3-4F. This would require a predictive paradigm and exquisite control over the molecular interaction and thermodynamic properties that have not been achieved yet. More than likely, an additional, high  $T_g$  component with suitable electronic structures that prevents BTP diffusion would be required to suppress diffusion and achieve improved stability.

The development of a BTP analog with a higher  $T_{\rm g}$  and lower diffusion coefficients is highly desirable to improve intrinsic stability. The required chains to achieve stability are so short that the modifications would severely impact solubility, processability, and performance. Our results point out an unresolved molecular design challenge and suggest a new family of NFA with an intrinsically high  $T_{\rm g}$  or an improved stabilization protocol needs to be discovered or developed to achieve high performance (>18%) and high stability at the same time <sup>58</sup>. More stable systems based on IT-M and IEICO-4F have  $T_{\rm g}$  of ~ 160 °C and ~ 190 °C, respectively, temperatures that represent in suitable target for new molecules. The molecular design



principles that give the ITIC and IEICO family of NFAs a higher  $T_{\rm g}$  need to be revealed and understood. The contribution due to molecular shape, size, stiffness, conformational entropy, branched versus unbranched, and arylated versus alkylated side-chains need to be disentangled. The analysis protocol developed and utilized here will allow to do so if a sufficient diversity of materials is utilized. Such insight would allow to design a core not only for desirable electronic properties, but also with a desired  $T_{\rm g}$  and thus stability. Regarding multicomponent inks that improve stability of low  $T_{\rm g}$  NFAs, the requirement to maintain percolation and the requirement to prevent diffusion will likely have to be met by two specifically engineered additives/acceptors. The complex solubility-fabrication-performance-stability parameter space and its intrinsic trade-offs are likely of relevance to all solution processed organic optoelectronic applications.

# EXPERIMENTAL PROCEDURES

#### Materials

PM6 (Mn: 24.2 kDa; Mw: 88.0 kDa; PDI: 3.361), BTP-eC7 and BTP-eC11 is provided by Hou group. BTP-4F-DT is provided by Nguyen group. BTP-C3-4F and BTP-4F was purchased from eFlexPV, BTP-eC9 was purchased from 1-Materials. All the solvents and other materials were purchased from commercial sources and used without further purification. The full names of materials mentioned in this study are listed in Supplemental Information.

#### Device Fabrication and Characterizations.

The performance for the devices was achieved after extensive optimization with an inverted structure of ITO/ZnO/Active layer/MoO<sub>3</sub>/Al, and the details are as follows. Prepatterned ITO-coated glass with a sheet resistance of  $\sim 15\Omega/\text{sq}$ . The Active layer was prepared following the previous study<sup>11</sup>. All cells were measured inside the glovebox. For device characterizations, J-V characteristics were measured under AM1.5G light (100mW cm<sup>-2</sup>) using a ClassAAA Newport solar simulator. The light intensity was calibrated using a standard Si diode (with KG5 filter,purchased from PV Measurement) to bring spectral mismatch to unity. J-V characteristics were recorded using a Keithley 236 source meter unit.

# **GIWAXS** Characterization.

GIWAXS was performed at the beamline 7.3.3, Advanced Light Source (ALS), Lawrence Berkeley National Laboratory. The samples were measured in a helium environment to minimize airscattering using 10 keV energy X-rays, which was incident at a grazing angle of 0.13°. The scattered X-rays were detected using a Pilatus 2M photon-counting detector. The sample to detector distance was 280 mm, which is calibrated from diffraction peaks of Silver-Behenate. Data analysis was performed using the NIKA package supported in the Igor Pro environment.

# Secondary Ion Mass Spectroscopy Measurements.

For depth profiles acquired in this study, ToF-SIMS experiments were conducted using a TOF SIMS V (ION TOF, Inc. Chestnut Ridge, NY) instrument equipped with a Bi<sup>3+</sup> liquid metal-ion gun, Cesium sputtering gun, and an electron flood gun for charge compensation. Cs<sup>+</sup> was used as the sputter source with a 10 keV energy and 24 nA current. The sputter area was 50 by 50 mm. The analysis chamber pressure was maintained below  $5.0 \times 10^{-9}$  mbar to avoid contamination of the surfaces to be analyzed.

# **AUTHOR CONTRIBUTIONS**

H.A. conceived the scientific framework with the help of Y.Q. Y.Q. designed the experimental protocols, coordinated the experimental work, made ToF-SIMS samples and wrote the manuscript with the input of H.A. J.H. provided the materials. Z.P. performed the ToF-SIMS measurements and analysis. A. G., S. K., and A. B. performed the TPV, CELIV and CE measurements. I. A analyzed GIWAXS data. N. B provided the DSC and VASE data of  $PC_{71}BM$  and  $T_{g}$  prediction calculation. All authors provided comments on the manuscript and contributed to the editing. H.A. and J.H. directed the study.



#### **CONFLICTS OF INTEREST**

The authors declare no competing financial interest.

#### **ACKNOWLEDGMENTS**

The authors gratefully acknowledge support from the US Office of Naval Research (ONR, grant no. N000142012155) and NSF INFEWS (CBET 1639429). J. H. acknowledges the support from the National Natural Science Foundation of China (NSFC, 21835006, 91633301, 51961135103, 51961165102, and 51673201). ToF-SIMS was performed at the Analytical Instrumentation Facility (AIF) at NCSU, which is partially supported by the State of North Carolina and the National Science Foundation. X-ray data were acquired at beamlines 7.3.3 at the ALS, which is supported by the Director, Office of Science, Office of Basic Energy Sciences, of the US Department of Energy under contract no. DE-AC02-05CH11231. Zhu, C., Schaible, E., Hexemer, A. and Wang, C. of the ALS(DOE) are acknowledged for assisting with the experimental setup and providing instrument maintenance. Du, Z. and Nguyen, T.-Q. are acknowledged for providing the BTP-4F-DT acceptor.

## REFERENCES AND NOTES

- 1. Yuan, J., Zhang, Y., Zhou, L., Zhang, G., Yip, H.-L., Lau, T.-K., Lu, X., Zhu, C., Peng, H., Johnson, P. A., Leclerc, M., Cao, Y., Ulanski, J., Li, Y., Zou, Y. (2019). Single-Junction Organic Solar Cell with over 15% Efficiency Using Fused-Ring Acceptor with Electron-Deficient Core. Joule 3, 1140-1151.
- Yao, H.,Cui, Y.,Qian, D.,Ponseca, C. S., Jr.,Honarfar, A.,Xu, Y.,Xin, J.,Chen, Z.,Hong, L.,Gao, B.,Yu, R.,Zu, Y.,Ma, W.,Chabera, P.,Pullerits, T.,Yartsev, A.,Gao, F., Hou, J.(2019).14.7% Efficiency Organic Photovoltaic Cells Enabled by Active Materials with a Large Electrostatic Potential Difference. J. Am. Chem. Soc. 141, 7743-7750.
- 3. Lin, Y., Wang, J., Zhang, Z. G., Bai, H., Li, Y., Zhu, D., Zhan, X. (2015). An electron acceptor challenging fullerenes for efficient polymer solar cells. Adv. Mater. 27, 1170-4.
- 4. Li, S.,Liu, W.,Shi, M.,Mai, J.,Lau, T.-K.,Wan, J.,Lu, X.,Li, C.-Z., Chen, H.(2016). A spirobifluorene and diketopyrrolopyrrole moieties based non-fullerene acceptor for efficient and thermally stable polymer solar cells with high open-circuit voltage. Energy Environ. Sci. 9, 604-610.
- Liu, S., Yuan, J., Deng, W., Luo, M., Xie, Y., Liang, Q., Zou, Y., He, Z., Wu, H., Cao, Y. (2020). High-efficiency organic solar cells with low non-radiative recombination loss and low energetic disorder Nat. Photon. 14, 300-305.
  Song, J., Li, C., Zhu, L., Guo, J., Xu, J., Zhang, X., Weng, K., Zhang, K., Min, J., Hao, X., Zhang, Y., Liu, F., Sun,
- o. Song, J., Li, C., Zhu, L., Guo, J., Xu, J., Zhang, A., Weng, K., Zhang, K., Will, J., Fiao, A., Zhang, T., Liu, F., Sun, Y. (2019). Ternary Organic Solar Cells with Efficiency > 16.5% Based on Two Compatible Nonfullerene Acceptors. Adv. Mater, 31, e1905645.
- 7. Qin, J.,An, C.,Zhang, J.,Ma, K.,Yang, Y.,Zhang, T.,Li, S.,Xian, K.,Cui, Y.,Tang, Y.,Ma, W.,Yao, H.,Zhang, S.,Xu, B.,He, C., Hou, J.(2020).15.3% efficiency all-small-molecule organic solar cells enabled by symmetric phenyl substitution. Sci. China Mater. 63, 1142-1150.
- 8. Liu, Q., Jiang, Y., Jin, K., Qin, J., Xu, J., Li, W., Xiong, J., Liu, J., Xiao, Z., Sun, K., Yang, S., Zhang, X., Ding, L.(2020).18% Efficiency organic solar cells. Sci. Bull. 65, 272-275.
- 9. Arunagiri, L.,Peng, Z.,Zou, X.,Yu, H.,Zhang, G.,Wang, Z.,Lin Lai, J. Y.,Zhang, J.,Zheng, Y.,Cui, C.,Huang, F.,Zou, Y.,Wong, K. S.,Chow, P. C. Y.,Ade, H., Yan, H.(2020).Selective Hole and Electron Transport in Efficient Quaternary Blend Organic Solar Cells, Joule 4, 1790-1805.
- 10. Yao, J., Qiu, B., Zhang, Z. G., Xue, L., Wang, R., Zhang, C., Chen, S., Zhou, Q., Sun, C., Yang, C., Xiao, M., Meng, L., Li, Y. (2020). Cathode engineering with perylene-diimide interlayer enabling over 17% efficiency single-junction organic solar cells. Nat. Commun. 11, 2726.
- 11. Qin, Y.,Xu, Y.,Peng, Z.,Hou, J., Ade, H.(2020).Low Temperature Aggregation Transitions in N3 and Y6 Acceptors Enable Double-Annealing Method That Yields Hierarchical Morphology and Superior Efficiency in Nonfullerene Organic Solar Cells. Adv. Funct. Mater. 2005011.
- 12. Cui, Y., Yao, H., Zhang, J., Xian, K., Zhang, T., Hong, L., Wang, Y., Xu, Y., Ma, K., An, C., He, C., Wei, Z., Gao, F., Hou, J. (2020). Single-Junction Organic Photovoltaic Cells with Approaching 18% Efficiency Adv. Mater. 32, e1908205.
- 13. Jiang, K., Wei, Q., Lai, J. Y. L., Peng, Z., Kim, H. K., Yuan, J., Ye, L., Ade, H., Zou, Y., Yan, H. (2019). Alkyl Chain Tuning of Small Molecule Acceptors for Efficient Organic Solar Cells. Joule 3, 3020-3033.
- 14. Zhang, M., Zhu, L., Zhou, G., Hao, T., Qiu, C., Zhao, Z., Hu, Q., Larson, B. W., Zhu, H., Ma, Z., Tang, Z., Feng, W., Zhang, Y., Russell, T. P., Liu, F. (2021). Single-layered organic photovoltaics with double cascading charge transport pathways: 18% efficiencies. Nat. Commun. 12, 309.
- Mulligan, C. J., Wilson, M., Bryant, G., Vaughan, B., Zhou, X., Belcher, W. J., Dastoor, P. C. (2014). A projection of commercial-scale organic photovoltaic module costs. Sol. Energy Mater Sol. Cells. 120, 9-17.
- Azzopardi, B., Emmott, C. J. M., Urbina, A., Krebs, F. C., Mutale, J., Nelson, J. (2011). Economic assessment of solar electricity production from organic-based photovoltaic modules in a domestic environment. Energy Environ. Sci. 4, 3741.
- 17. Liao, C., Chen, Y., Lee, C., Wang, G., Teng, N., Lee, C., Li, W., Chen, Y., Li, C., Ho, H., Tan, P. H., Wang, B., Huang. Y., Young, R., Wasielewski, M. R., Marks, T. B., Chang, Y., Facchetti, A.(2020). Processing Strategies

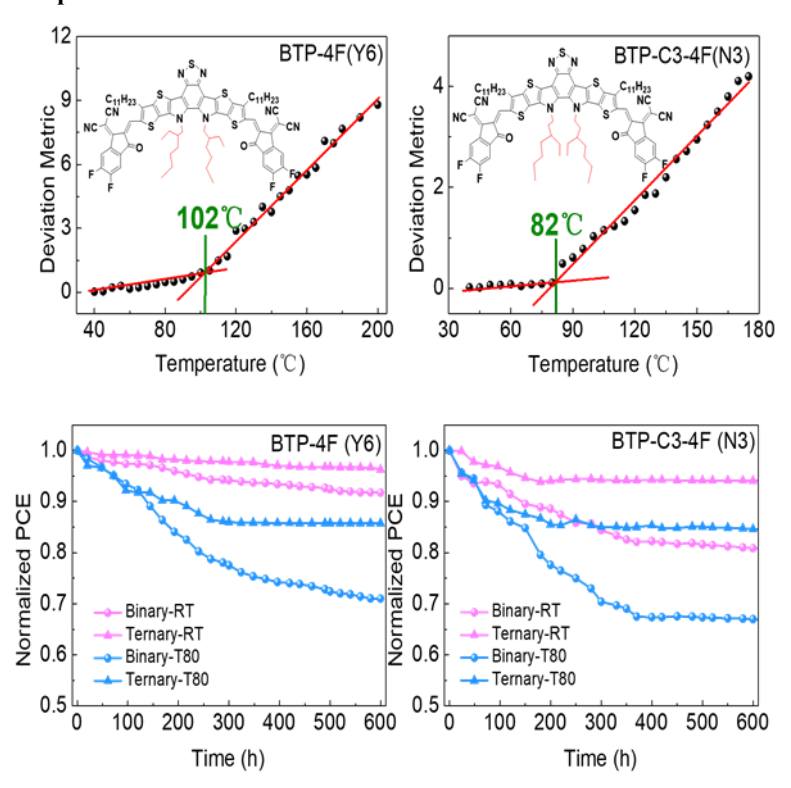


- for an Organic Photovoltaic Module with over 10% Efficiency. Joule. 4, 189-206 18. Sun, R., Wu, Q., Guo, J., Wang, T., Wu, Y., Qiu, B., Luo, Z., Yang, W., Hu, Z., Guo, J., Shi, M., Yang, C., Huang, F., Li, Y., Min, J.(2020). A Layer-by-Layer Architecture for Printable Organic Solar Cells Overcoming the Scaling Lag of Module Efficiency. Joule. 4, 407-419
- 19. Du, X., Heumueller, T., Gruber, W., Almora, O., Classen, A., Qu, J., He, F., Unruh, T., Li, N., Brabec, C. J. (2020). Unraveling the Microstructure-Related Device Stability for Polymer Solar Cells Based on Nonfullerene Small-Molecular Acceptors. Adv. Mater. 32, e1908305.
- 20. Du, X., Heumueller, T., Gruber, W., Classen, A., Unruh, T., Li, N., Brabec, C. J. (2019). Efficient Polymer Solar Cells Based on Non-fullerene Acceptors with Potential Device Lifetime Approaching 10 Years, Joule 3, 215-226. 21. Baran, B., Gasparini, N., Wadsworth, A., Tan, C., Wehbe, N., Song, X., Hamid, Z., Zhang, W., Neophytou, M., Kirchartz, T., Brabec, C., Durrant, J., McCulloch, I. (2018). Robust nonfullerene solar cells approaching unity external quantum efficiency enabled by suppression of geminate recombination. Nat. Commun. 9, 2059
- Savagatrup, S., Printz, A. D., O'Connor, T. F., Zaretski, A. V., Rodriquez, D., Sawyer, E. J., Rajan, K. M., Acosta, R. I., Root, S. E., Lipomi, D. J. (2015). Mechanical degradation and stability of organic solar cells: molecular and microstructural determinants. Energy Environ. Sci. 8, 55-80.
- 23. Drakonakis, V. M.,Savva, A.,Kokonou, M., Choulis, S. A.(2014).Investigating electrodes degradation in organic photovoltaics through reverse engineering under accelerated humidity lifetime conditions. Sol. Energy Mater Sol. 130, 544-550.
- 24. Glen, T. S., Scarratt, N. W., Yi, H., Iraqi, A., Wang, T., Kingsley, J., Buckley, A. R., Lidzey, D. G., Donald, A. M. (2016). Dependence on material choice of degradation of organic solar cells following exposure to humid air. J Polym Sci B Polym Phys. 54, 216-224.
- 25. Manceau, M.,Bundgaard, E.,Carlé, J. E.,Hagemann, O.,Helgesen, M.,Søndergaard, R.,Jørgensen, M., Krebs, F. C.(2011). Photochemical stability of  $\pi$ -conjugated polymers for polymer solar cells: a rule of thumb. J. Mater. Chem. A 21, 4132.
- Seemann, A., Sauermann, T., Lungenschmied, C., Armbruster, O., Bauer, S., Egelhaaf, H. J., Hauch, J. (2011). Reversible and irreversible degradation of organic solar cell performance by oxygen. Solar Energy 85, 1238-1249.
- 27. Turak, A.(2013).Interfacial degradation in organic optoelectronics. RSC Advances 3, 6188.
- 28. Zhu, Y., Gadisa, A., Peng, Z., Ghasemi, M., Ye, L., Xu, Z., Zhao, S., Ade, H. (2019). Rational Strategy to Stabilize an Unstable High-Efficiency Binary Nonfullerene Organic Solar Cells with a Third Component. Adv. Energy Mater. 9, 1900376.
- 29. Zhang, C., Heumueller, T., Leon, S., Gruber, W., Burlafinger, K., Tang, X., Perea, J. D., Wabra, I., Hirsch, A., Unruh, T., Li, N., Brabec, C. J. (2019). A top-down strategy identifying molecular phase stabilizers to overcome microstructure instabilities in organic solar cells. Energy Environ. Sci. 12, 1078-1087.
- 30. Heumueller, T.,Mateker, W. R.,Sachs-Quintana, I. T.,Vandewal, K.,Bartelt, J. A.,Burke, T. M.,Ameri, T.,Brabec, C. J., McGehee, M. D.(2014).Reducing burn-in voltage loss in polymer solar cells by increasing the polymer crystallinity. Energy Environ. Sci. 7, 2974-2980.
- 31. Ye, L., Li, S., Liu, X., Zhang, S., Ghasemi, M., Xiong, Y., Hou, J., Ade, H. (2019). Quenching to the Percolation Threshold in Organic Solar Cells. Joule 3, 443-458.
- 32. Ghasemi, M.,Hu, H.,Peng, Z.,Rech, J. J.,Angunawela, I.,Carpenter, J. H.,Stuard, S. J.,Wadsworth, A.,McCulloch, I.,You, W., Ade, H.(2019).Delineation of Thermodynamic and Kinetic Factors that Control Stability in Non-fullerene Organic Solar Cells. Joule 3, 1328-1348.
- 33. Yu, L., Qian, D., Marina, S., Nugroho, F. A. A., Sharma, A., Hultmark, S., Hofmann, A. I., Kroon, R., Benduhn, J., Smilgies, D. M., Vandewal, K., Andersson, M. R., Langhammer, C., Martin, J., Gao, F., Muller, C. (2019). Diffusion-Limited Crystallization: A Rationale for the Thermal Stability of Non-Fullerene Solar Cells. ACS Appl. Mater. Interfaces. 11, 21766-21774.
- 34. Hu, H., Ghasemi, M., Peng, Z., Zhang, J., Rech, J. J., You, W., Yan, H., Ade, H. (2020). The Role of Demixing and Crystallization Kinetics on the Stability of Non-Fullerene Organic Solar Cells. Adv. Mater. e2005348.
- 35. Ghasemi, M.,Balar, N.,Peng, Z.,Hu, H.,Qin, Y.,Kim, T.,Rech, J. J.,Bidwell, M.,Mask, W.,McCulloch, I.,You, W.,Amassian, A.,Risko, C., O'Connor, B. T., Ade, H.(2021). A molecular interaction-diffusion framework for predicting organic solar cell stability. Nat. Mater. https://doi.org/10.1038/s41563-020-00872-6
- 36. Ye, L., Collins, B. A., Jiao, X., Zhao, J., Yan, H., Ade, H. (2018). Miscibility-Function Relations in Organic Solar Cells: Significance of Optimal Miscibility in Relation to Percolation. Adv. Energy Mater. 8, 1703058.
- 37. Ye, L., Hu, H., Ghasemi, M., Wang, T., Collins, B. A., Kim, J. H., Jiang, K., Carpenter, J. H., Li, H., Li, Z., McAfee, T., Zhao, J., Chen, X., Lai, J. L. Y., Ma, T., Bredas, J. L., Yan, H., Ade, H. (2018). Quantitative relations between interaction parameter, miscibility and function in organic solar cells. Nat. Mater. 17, 253-260.
- 38. Li, N.,Perea, J. D.,Kassar, T.,Richter, M.,Heumueller, T.,Matt, G. J.,Hou, Y.,Guldal, N. S.,Chen, H.,Chen, S.,Langner, S.,Berlinghof, M.,Unruh, T., Brabec, C. J.(2017).Abnormal strong burn-in degradation of highly efficient polymer solar cells caused by spinodal donor-acceptor demixing. Nat. Commun. 8, 14541.
- 39. Peng, Z., Jiao, X., Ye, L., Li, S., Rech, J. J., You, W., Hou, J., Ade, H. (2018). Measuring Temperature-Dependent Miscibility for Polymer Solar Cell Blends: An Easily Accessible Optical Method Reveals Complex Behavior. Chem. Mater. 30, 3943-3951.
- Standard Test Methods for Photovoltaic Modules in Cyclic Temperature and Humidity Environments, ASTM Standard E 1171.
- 41. Liao, Q., Kang, Q., Yang, Y., Zheng, Z., Qin, J., Xu, B., Hou, J. (2021) Highly Stable Organic Solar Cells Based on an Ultraviolet-Resistant Cathode Interfacial Layer. CCS Chemistry. https://doi.org/10.31635/ccschem.021.202100852
- 42. Liu, H., Liu, Z., Wang, S., Huang, J., Ju, H., Chen, Q., Yu, J., Chen, H., Li, C. (2019) Boosting Organic–Metal Oxide Heterojunction via Conjugated Small Molecules for Efficient and Stable Nonfullerene Polymer Solar Cells Adv. Energy Mater. 1900887



- 43. Collins, B. A.,Li, Z.,Tumbleston, J. R.,Gann, E.,McNeill, C. R., Ade, H.(2013). Absolute Measurement of Domain Composition and Nanoscale Size Distribution Explains Performance in PTB7:PC71BM Solar Cells. Adv. Energy Mater. 3, 65-74.
- 44. Gann, E., Young, A. T., Collins, B. A., Yan, H., Nasiatka, J., Padmore, H. A., Ade, H., Hexemer, A., Wang, C. (2012). Soft x-ray scattering facility at the Advanced Light Source with real-time data processing and analysis. Rev. Sci. Instrum. 83, 045110.
- 45. Hexemer, A.,Bras, W.,Glossinger, J.,Schaible, E.,Gann, E.,Kirian, R.,MacDowell, A.,Church, M.,Rude, B., Padmore, H.(2010). A SAXS/WAXS/GISAXS Beamline with Multilayer Monochromator. J Phys Conf Ser. 247, 012007
- 46. Jiao, X., Ye, L. Ade, H. (2017). Quantitative Morphology-Performance Correlations in Organic Solar Cells: Insights from Soft X-Ray Scattering. Adv. Energy Mater. 7, 1700084.
- 47. Gasparini, N., Jiao, X., Heumueller, T., Baran, D., Matt, G, J., Fladischer, S., Spiecker, E., Ade, H., Brabec, C, J., Ameri, T. (2016) Designing ternary blend bulk heterojunction solar cells with reduced carrier recombination and a fill factor of 77%. Nat. Energy. 1, 16118.
- 48. Kawashima, K., Tamai, Y., Ohkita, H., Osaka, I., Takimiya, K. (2015). High-efficiency polymer solar cells with small photon energy loss. Nat. Commun. 6, 10085.
- Bartesaghi, D., Perez Idel, C., Kniepert, J., Roland, S., Turbiez, M., Neher, D., Koster, L. J. (2015). Competition between recombination and extraction of free charges determines the fill factor of organic solar cells. Nat. Commun. 6, 7083
- 50. Bartelt, J.A., Beiley, Z.M., Hoke, E.T., Mateker, W.R., Douglas, J.D., Collins, B.A., Tumbleston, J.R., Graham, K.R., Amassian, A., Ade, H., et al. (2013). The importance of fullerene percolation in the mixed regions of polymer-fullerene bulk heterojunction solar cells. Adv. Energy Mater. 3, 364–374.
- 51. Reimschuessel, H. K., (1979). On the Glass Transition Temperature of Comblike Polymers: Effects of Side Chain Length and Backbone Chain Structure. J Polym Sci A Polym Chem, 17, 2447-2457
- 52. Qian, Z.,Cao, Z.,Galuska, L.,Zhang, S.,Xu, J., Gu, X.(2019). Glass Transition Phenomenon for Conjugated Polymers. Macromol Chem Phys 220, 1900062.
- 53. J. M. Barrales-Rienda, J. Gonzdlez Ramos, J. G., Chaves, M. S. (1997) Glass Transition Temperatures of Poly N-(n-alkyl)-maleimides. British Polym J. https://doi.org/10.1002/pi.4980090103
- 54. Pankaj, S., Hempel, E., Beiner, M. (2009) Side-Chain Dynamics and Crystallization in a Series of Regiorandom Poly(3-alkylthiophenes). Macromolecules. 42, 716-724
- 55. Müller, C.(2015). On the Glass Transition of Polymer Semiconductors and Its Impact on Polymer Solar Cell Stability. Chem. Mater. 27, 2740-2754.
- 56. Xie, R., Weisen, A. R., Lee, Y., Aplan, M. A., Fenton, A. M., Masucci, A. E., Kempe, F., Sommer, M., Pester, C. W., Colby, R. H., Gomez, E. D.(2020). Glass transition temperature from the chemical structure of conjugated polymers. Nat. Commun 11, 893
- 57. Laredo, E., Suarez, N., Bello, A., Marquez, L.(1996). The glass transition in linear low density polyethylene determined by thermally stimulated depolarization currents. J Polym Sci B Polym Phys. 34, 641-648
- 58. Zhang, J., Tan, H., Guo, X., Facchetti, A., Yan, H. (2018). Material insights and challenges for non-fullerene organic solar cells based on small molecular acceptors. Nat. Energy 3, 720-31

# **Graphical Abstract**



# eTOC Blurb

We determine the thermal transition temperatures ( $T_{\rm g}$ ) of seven BTP-based non-fullerene acceptors and have developed a structure- $T_{\rm g}$  framework. We also show that PC71BM has a miscibility above the percolation threshold in PM6 and can thus maintain local charge percolation. However, PC71BM is not miscible with BTP-C3-4F and can thus not prevent BTP-C3-4F diffusion and the unfavorable vertical gradients that still degrades performance, high Tg component with suitable electronic structures that prevents BTP diffusion would be required to achieve commercial viability.